Pt-Catalyzed Growth of Ni Nanoparticles in Aqueous CTAB Solution

Marek Grzelczak,*,† Jorge Pérez-Juste,† Benito Rodríguez-González,† Marina Spasova,‡ Igor Barsukov,‡ Michael Farle,‡ and Luis M. Liz-Marzán*,†

Departamento de Química Física, Universidade de Vigo, 36310, Vigo, Spain, and Fachbereich Physik and Center for Nanointegration, Universität Duisburg-Essen, D-47048 Duisburg, Germany

Received March 6, 2008. Revised Manuscript Received April 28, 2008

NiO-passivated nickel nanoparticles were grown on small platinum seeds, which served as catalysts for the reduction of Ni^{2+} with hydrazine, in aqueous solutions of the cationic surfactant cetyltrimethylammonium bromide. Control of particle size was achieved through manipulation of the reduction conditions, among which the molar ratio between nickel salt and platinum seeds was found to be dominant. HRTEM, XPS, and XRD show the polycrystaline structure of the particles and the presence of metallic Ni, as well as NiO_x and $Ni(OH)_2$. The magnetic properties were studied as a function of size and reveal superparamagnetic response at room temperature for 14 nm diameter nanoparticles and ferromagnetic behavior for the nanoparticles with diameters larger than 24 nm. The ferromagnetic nature of bigger Ni particles was found to induce chain formation, even in the absence of external magnetic fields, which is demonstrated through in situ coating with silica, which results in fossilized nanoparticle chains. Additionally, we propose a mechanism for the growth of nickel on the platinum nanoparticle seeds surface.

Introduction

The interesting magnetic properties of metallic nickel have driven intense research activities toward nanoparticle synthesis, looking in particular for a high degree of control over size and shape,[1–4] because of the related possibility to control the magnetic anisotropy, and the subsequent potential application in 2D or 3D assembly. Ni/NiO nanocrystals have been shown to find applications as anode materials for rechargeable batteries, ethanol fuel cells, and electrochemical capacitors.[5] In the past decade, the most successful procedures for the synthesis of monodisperse magnetic nanoparticles have involved the one-pot decomposition of organometallic precursors at high temperature.[6–8] However, both Sun[9] and Philipse[10] proposed the organometallic seeded-growth method for the synthesis of iron oxide, with a fine control of the final particle size between 4 and 20 nm. To the best of our knowledge, no effort has been made toward the synthesis of nickel particles in aqueous solution using seed-mediated methods. On the other hand, a number of papers have reported the hydroxide forced, aqueous synthesis of nickel nanoparticles by hydrazine reduction and stabilization with a cationic surfactant (cetyltrimethylammonium bromide, CTAB),[11–14] where the particle size was controlled to a certain extent through the molar ratio between Ni(II) and hydrazine.[15] On the basis of the experience in our group for CTAB-assisted seeded-growth of various types of gold nanoparticles,[16] as well as for the catalytic growth of metallic Ni on platinum seeds, supported either on gold nanorods[17] or on carbon nanotubes,[18] we have developed and optimized the growth of reasonably monodisperse nickel nanoparticles on individual platinum seeds, in the presence of CTAB, with the possibility of controlling the average particle size in the range between 13 and 33 nm. Upon a postsynthetic washing procedure, air-stable Ni nanoparticles were obtained, because of surface passivation, so that they could be easily handled under external magnetic fields, and functionalized through coating with silica. Magnetic characterization of these particles shows a ferromagnetic behavior, which is maintained at room temperature for those with bigger sizes, which

* Corresponding author. E-mail: lmarzan@uvigo.es.
† Universidade de Vigo.
‡ Universitat Duisburg-Essen.

(1) Park, J.; Kang, E.; Son, S. U.; Park, H. M.; Lee, M. K.; Kim, J.; Kim, K. W.; Noh, H.-J.; Park, J.-H.; Bae, C. J.; Park, J.-G.; Hyeon, T. *Adv. Mater.* **2005**, *17*, 429.
(2) Cordente, N.; Respaud, M.; Senocq, F.; Casanove, M.-J.; Amiens, C.; Chaudret, B. *Nano Lett.* **2001**, *1*, 565.
(3) Leng, Y.; Li, Y.; Li, X.; Takahashi, S. *J. Phys. Chem. C* **2007**, *111*, 6630.
(4) Ung, D.; Soumare, Y.; Chakroune, N.; Viau, G.; Vaulay, M. J.; Richard, V.; Fievet, F. *Chem. Mater.* **2007**, *19*, 2084.
(5) Parada, C.; Moran, E. *Chem. Mater.* **2006**, *18*, 2719.
(6) Lu, A. H.; Salabas, E. L.; Schueth, F. *Angew.Chem., Int. Ed.* **2007**, *46*, 1222.
(7) Jeong, U.; Teng, X.; Wang, Y.; Yang, H.; Xia, Y. *Adv. Mater.* **2007**, *19*, 33.
(8) Huber, D. L. *Small* **2005**, *1*, 482.
(9) Sun, S.; Zeng, H. *J. Am. Chem. Soc.* **2002**, *124*, 8204.
(10) Klokkenburg, M.; Vonk, C.; Claesson, E. M.; Meeldijk, J. D.; Erne, B. H.; Philipse, A. P. *J. Am. Chem. Soc.* **2004**, *126*, 16706.
(11) Chen, D.-H.; Wu, S.-H. *Chem. Mater.* **2000**, *12*, 1354.
(12) Zhang, D. E.; Ni, X. M.; Zheng, H. G.; Li, Y.; Zhang, X. J.; Yang, Z. P. *Mater. Lett.* **2005**, *59*, 2011.
(13) Wu, S.-H.; Chen, D.-H. *Chem. Lett.* **2004**, *33*, 406.
(14) Chen, D.-H.; Hsieh, C.-H. *J.Mater.Chem.* **2002**, *12*, 2412.
(15) Boudjahem, A.-G.; Monteverdi, S.; Mercy, M.; Bettahar, M. M. *Langmuir* **2004**, *20*, 208.
(16) Rodríguez-Fernández, J.; Pérez-Juste, J.; García de Abajo, F. J.; Liz-Marzán, L. M. *Langmuir* **2006**, *22*, 7007.
(17) Grzelczak, M.; Rodríguez-González, B.; Pérez-Juste, J.; Liz-Marzán, L. M. *Adv. Mater.* **2007**, *19*, 2262.
(18) Grzelczak, M.; Correa-Duarte, M. A.; Salgueiriño-Maceira, V.; Rodríguez-González, B.; Rivas, J.; Liz.Marzán, L. M. *Angew. Chem., Int. Ed.* **2007**, *46*, 7026.

10.1021/cm800665s CCC: $40.75
Published on Web 07/23/2008

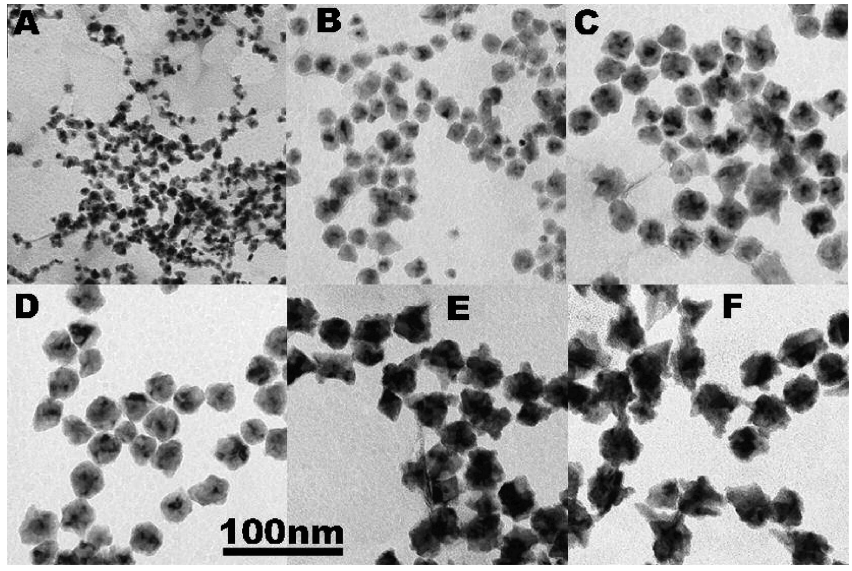

Figure 1. TEM images of nickel nanoparticles prepared with different amounts of platinum seed. The Ni^{2+}/Pt^0 molar ratios used for the different samples were 10, 20, 30, 40, 80, and 100, for images A−F, respectively.

could be directly observed through both spontaneous (zero-field) and field-induced chain formation (both on surfaces and in solution) because of interactions between permanent magnetic dipoles.

Experimental Section

Chemicals. Cetyltrimethylammonium bromide (CTAB) 95%, potassium tetrachloroplatinate(II) (K_2PtCl_4), sodium borohydride ($NaBH_4$), nickel (II) chloride hexahydrate ($NiCl_2 \cdot 6H_2O$), and hydrazine (N_2H_4) 64%, were purchased from Aldrich and used as received. Milli-Q water with a resistivity higher than 18.2 MΩ cm was used in all of the preparations.

Synthesis of Platinum Seeds. To 9.63 mL of 0.1 M CTAB solution was added 50 μL of 0.05 M K_2PtCl_4. The mixture was heated up to 40 °C for about 5 min until the solution became clear. The vial was capped immediately after adding 0.3 mL of 0.06 M $NaBH_4$. After 10 min, the vial was opened and stirred for several minutes until all sodium borohydride was decomposed.

Nickel Growth. In a typical synthesis, aqueous solutions of $NiCl_2$ (0.5 mM) and N_2H_4 (15 mM) were mixed with various amounts of Pt seed solution (2, 1, 0.66, 0.5, 0.25, 0.2 mL). The total volume of the solution was fixed at 10 mL and the final CTAB concentration was 20 mM in all samples. The solution was maintained for 2−3 h at 40 °C and the product was centrifuged several times at 8000 rpm for 30 min and redispersed in water.

Characterization. Transmission electron microscopy (TEM) images were obtained with a JEOL JEM 1010 transmission electron microscope operating at an acceleration voltage of 100 kV, whereas high-resolution TEM (HRTEM) was performed with a JEOL JEM 2010F operating at an acceleration voltage of 200 kV. Scanning electron microscopy (SEM) images were obtained in a JEOL JSM-6700F FEG scanning electron microscope operating at an acceleration voltage of 15 kV for secondary-electron imaging (SEI) and at 10 kV for backscattering-electron imaging (YAG detector). XPS analysis of the samples was performed using a VG Escalab 250 iXL ESCA instrument (VG Scientific), equipped with aluminum Kα1.2 monochromatic radiation at 1486.92 eV X-ray source.

Results and Discussion

Morphological Characterization and Size Control. In all earlier reports on the reduction of Ni(II) by hydrazine in CTAB solution, it was indicated that basic pH was a necessary condition. It was additionally indicated that, although the size of the particles could be controlled by adjusting the Ni(II) to hydrazine molar ratio, uncontrolled nucleation processes resulted in a noticeable increase in polydispersity. However, it has been shown that introduction in the growth solution of a "nucleation agent" such as small amounts of silver,[19–21] platinum,[22] palladium,[23] or ruthenium[4] salts noticeably improves the quality of the formed particles. Apparently, small metallic seeds are formed when the salts are reduced by hydrazine, then promoting nickel reduction by the remaining hydrazine on the in situ formed seeds, which act as catalysts. The addition of the nucleation agent not only accelerates the nucleation of nickel particles but also leads to formation of smaller particles, with lower polydispersity. We therefore decided to use as-prepared tiny platinum nanoparticles as nucleation seeds, in a similar way to the use of gold seeds for gold nanorods synthesis. Although conventional size characterization (TEM) did not allow us to obtain reliable information about the diameter of Pt seeds, we estimate diameters around 1−2 nm, in agreement with those reported for Au seeds.[24]

The TEM images in Figure 1 illustrate the morphology of nickel particles obtained with different molar ratios between nickel (salt) and the platinum (seeds), as indicated in the caption. Analysis of the TEM images (minimum count of 70 particles) indicated that the average particle diameter could be varied between 13.73 ± 1.95 and 33.45 ± 3.70 nm, for $Ni^{2+}/Pt^0 = 10$ and 100, respectively. Size distributions for each sample can be seen in the Supporting Information (Figure S1) and confirm a continuous increase

(19) Li, Y. D.; Li, C. W.; Wang, H. R.; Li, L. Q.; Qian, Y. T. *Mater. Chem. Phys.* **1999**, *59*, 88.
(20) Chen, M.; Zhou, J.; Xie, L.; Gu, G.; Wu, L. *J. Phys. Chem. C* **2007**, *111*, 11829.
(21) Viau, G.; Fiévet-Vincent, F.; Fiévet, F. *Solid State Ionics* **1996**, *84*, 259.
(22) Li, D.; Komarneni, S. *J. Am. Ceram. Soc.* **2006**, *89*, 1510.
(23) Hegde, M. S.; Larcher, D.; Dupont, L.; Beaudoin, B.; Tekaia-Elhsissen, K.; Tarascon, J. M. *Solid State Ionics* **1997**, *93*, 33.
(24) Liu, M.; Guyot-Sionnest, P. *J.Phys. Chem. B* **2005**, *109*, 22192.

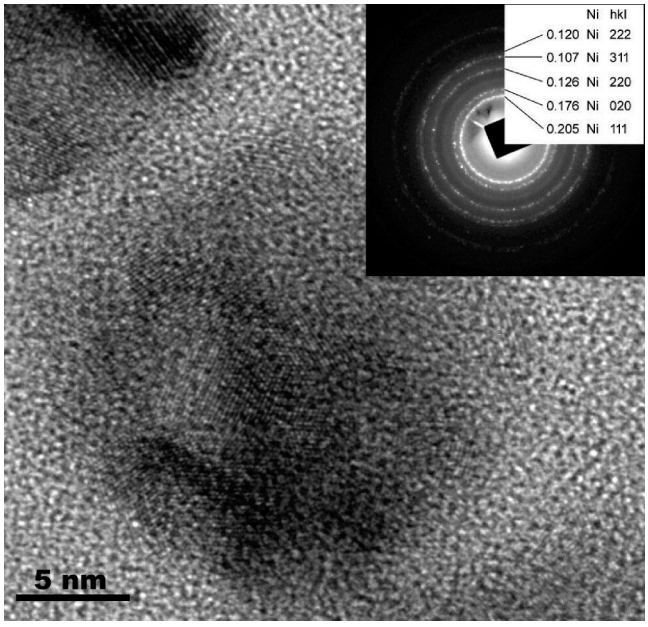

Figure 2. HRTEM image of a nickel nanoparticle (24 nm, Figure 1C), showing a polycrystalline structure, with 2−3 nm domains. In the inset, a SAED pattern from the same particle is shown, with indication of the corresponding interplanar distances.

of particle diameter with decreasing amount of platinum seeds, which was previously observed for the seeded-growth of gold nanoparticles.[25] The presence of a passivating oxide layer was confirmed by XPS, which revealed the presence of metallic nickel, nickel oxides (NiO_x), and nickel hydroxide- $Ni(OH)_2$ (see the Supporting Information, Figure S2), again in agreement with earlier reports.[26] Because complete oxidation of the particles was not observed over prolonged periods of time, we suggest that NiO_x covers the Ni surface, whereas the hydroxide is only present at the outermost layers. Additionally, the X-ray powder diffractogram (see the Supporting Information, Figure S3) of the as-prepared product shows two characteristic peaks corresponding to face-centered cubic (fcc) metallic nickel (ICSD 76667), as well as peaks that can be indexed to NiO_2 (ICSD 88720).

Complementary high-resolution TEM (HRTEM) characterization (Figure 2) of nickel nanoparticles from the sample shown in Figure 1C (Ni:Pt ratio 30), reveals a highly polycrystalline structure, with crystal domains about 2−3 nm. A better impression of the polycrystalline structure of the particles can be observed in dark-field mode, as shown in the Supporting Information (Figure S4), where bright and dark areas can be distinguished within each particle, corresponding to crystalline domains with different orientations. Unfortunately, this polycrystalline structure makes it impossible to identify the small Pt seeds, because of diffraction of the electrons on each domain while traveling through the particle. The selected area electron diffraction (SAED) pattern (Figure 2, inset) from a single particle confirms the presence of metallic nickel, since five interplanar distances can be identified, which are consistent with pure face-centered cubic (fcc) metallic nickel. It is interesting to note that, HRTEM images did not allow us to directly observe the protective oxide layer on the nanoparticles surface, suggesting that it is rather thin. On the basis of our previous work on Au@Ni rods,[17] we can estimate that the thickness of the oxide shell could correspond to one crystal domain, which is ca. 2−3nm.

Growth Mechanism. The synthesis of platinum seeds involves the complexation of Pt^{2+} with the surfactant (CTAB), leading to the formation of $(CTA)_2PtBr_4$ metallomicelles,[27] followed by reduction of Pt^{II} to Pt^0 with a strong reducing agent, sodium borohydride. Such Pt seeds are stabilized by a CTAB bilayer, which prevents their aggregation. As mentioned above, earlier reports showed that addition of a strong base, such as NaOH is required for reduction of nickel with hydrazine; however we found that this is not necessary when Pt seeds are present. Confirmation of the catalytic effect of Pt was achieved through a control experiment in which the same growth solution was prepared without Pt seeds, with the result that no nickel reduction was observed. This suggests that the available Pt surface is a key factor for initializing the reduction of nickel, which agrees with our earlier studies on Ni deposition on gold nanorods and carbon nanotubes.[17,18] However, since the TEM and HRTEM investigation did not allow us to identify the Pt cores inside Ni particles, we carried out a similar synthesis using bigger platinum nanoparticle seeds for nickel reduction. Figure 3A shows Pt nanoparticles prepared according to the experimental procedure discussed in ref,[28] with the presence of mainly cubic particles (9.00 nm side length) along with some larger, porous particles. Upon washing by centrifugation and redispersion in CTAB (see the Supporting Information for details), the prepared Pt particles were used as a seeds for nickel reduction by hydrazine in the presence of CTAB. After several hours, the color of the solution turned black, indicating the formation of nickel nanoparticles, which was confirmed by TEM (Figure 3B). Despite the polycrystalline structure of the nickel particles and the rough, oxidized surface, the presence of the Pt cores can be observed in most particles as central black spots. This control experiment shows that different types of platinum seeds can be used to reduce nickel in aqueous hydrazine solution, again in agreement with our earlier reports showing reduction of nickel on platinum-coated carbon nanotubes and gold nanorods.[17,18]

To understand the reduction process, it is important to remember that hydrazine can easily form complexes with transition metals.[29] However, in concentrated aqueous solutions, nickel−hydrazine complexes can exist as mixtures of $[Ni(N_2H_4)_2]Cl_2$, $[Ni(N_2H_4)_3]Cl_2$, and $[Ni(NH_3)_6]Cl_2$, whose compositions are highly dependent on reaction temperature and N_2H_5OH/Ni^{2+} molar ratio.[30,31] However, in the present synthetic approach, low Ni^{2+} concentrations (0.5 mM) were used, with a pale-green color, which upon mixing with

(25) Jana, N. R.; Gearheart, L.; Murphy, C. J. *Langmuir* **2001**, *17*, 6782.
(26) Grosvenor, A. P.; Biesinger, M. C.; Smart, R. S. C.; McIntyre, N. S. *Surf. Sci.* **2006**, *600*, 1771.
(27) Veisz, B.; Kiraly, Z. *Langmuir* **2003**, *19*, 4817.
(28) Lee, H.; Habas, S. E.; Kweskin, S.; Butcher, D.; Somorjai, G. A.; Yang, P. *Angew. Chem., Int. Ed.* **2006**, *45*, 7824.
(29) Bottomley, F. *Q. Rev. Chem. Soc.* **1970**, *24*, 617.
(30) Park, J. W.; Chae, E. H.; Kim, S. H.; Lee, J. H.; Kim, J. W.; Yoon, S. M.; Choi, J.-Y. *Mater. Chem. Phys.* **2006**, *97*, 371.
(31) Li, Y. D.; Li, L. Q.; Liao, H. W.; Wang, H. R. *J. Mater. Chem.* **1999**, *9*, 2675.

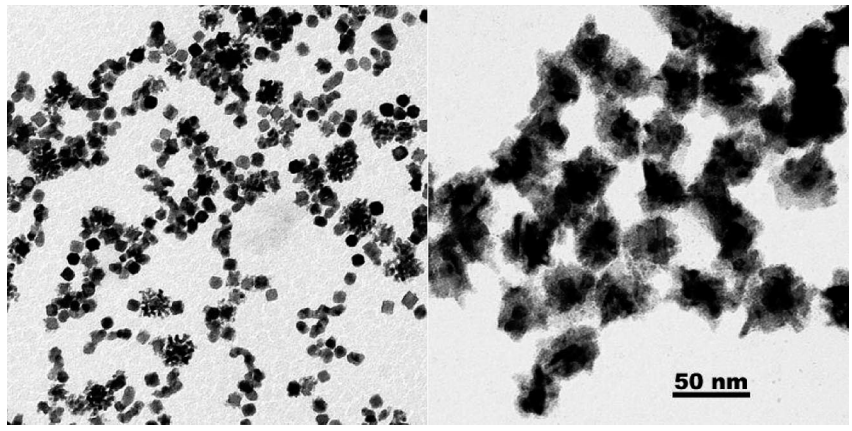

Figure 3. TEM micrographs of platinum nanocubes (A) with side length 9.00 nm, and nickel particles (B) grown on them. The final average dimension of Pt/Ni core/shell nanoparticles is 34.2 nm.

hydrazine (15 mM) turned blue-sky, corresponding to the $[Ni(N_2H_4)_2]Cl_2$ complex, which is very stable in ambient conditions.[32] The freshly prepared complex is then immediately used for nickel reduction in the presence of CTAB.

The presence of CTAB also seems to be important. Cetyltrimethylammonium bromide (CTAB) is a cationic surfactant, which has been widely used as stabilizer for the growth of gold nanoparticles in water, because of its ability to form bilayers, with the hydrophilic ammonium head groups pointing toward both the metal surface and solution.[33] Additionally, it has been found that an important factor for CTAB-assisted gold reduction is the formation of a complex between the metal precursor salt and CTAB, leading to the so-called "soft template mechanism".[34] Although in principle the cationic character of the nickel precursor (Ni^{2+}) and its complex with hydrazine $[Ni(N_2H_4)_2]^{2+}$, seems to prevent interaction with the surfactant (CTA^+Br^-), CTAB appears to be an essential ingredient for the stabilization of nickel particles, preserving the stability of Pt@CTAB seeds. On the other hand, in the present reaction conditions, the use of anionic stabilizers such as SDS or sodium citrate is excluded, most likely because of the possibility of becoming a counterion with the complex, which is insoluble in aqueous solution.

In previous works, it was shown that the $[Ni(N_2H_4)_2]Cl_2$ complex can be decomposed by OH^- groups at high temperature. We show here that in the presence of metallic platinum seeds, the initial reduction of nickel can take place at 40 °C. Under the used reaction conditions, the N_2H_5OH/Ni^{2+} molar ratio is about 30, so that most (uncomplexed) hydrazine is free in solution and can react with platinum. Indeed, it is well-known that hydrazine can be easily decomposed on the surface of Pt particles through formation of the electrophilic radicals, which can then react with other hydrazine molecules[35] or with $[Ni(N_2H_4)_2]Cl_2$ present in solution. Subsequent hydrazine decomposition on the surface of the reduced metal is facilitated,[36] thus favoring further

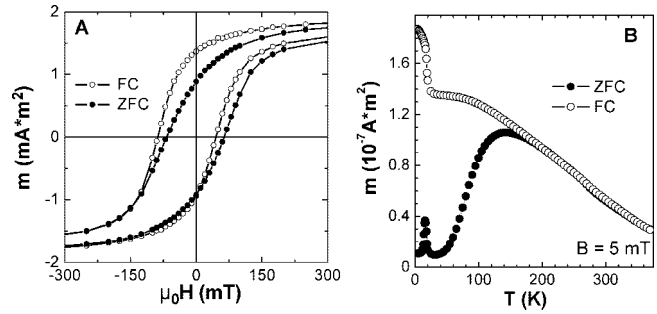

Figure 4. (A) Hysteresis loops of surface oxidized Ni nanoparticles of 33.5 nm diameter recorded at 2 K after cooling the sample in zero field (solid symbols) and in an applied field of 5 T (open symbols). (B) Temperature dependence of the ZFC (solid symbols) and FC (open symbols) magnetization of the 14 nm oxide-coated Ni nanoparticles. See the text for details.

Ni reduction. Another interesting feature is that the reduction of nickel is accompanied by gas evolution, which is obviously related to hydrazine decomposition, resulting in formation of N_2 and H_2.[35] It is remarkable that the reaction does not take place if the vessel is left open, suggesting that the produced gases are important to prevent the oxidation of nickel particles. Interestingly, decomposition of hydrazine on the Pt surface can be inhibited by electrosorption of heavy metals at the underpotential range, leading to the formation of a monolayer of the heavy metal (Pb, Cd, Tl).[37] We have indeed observed that reduction of Ni^{2+} did not occur when small amounts of $Pb(NO)_2$ were present in the growth solution, suggesting that Pb^{2+} could compete with Ni^{2+} reduction, leading to poisoning of the Pt seeds.

Magnetic Characterization. The magnetic properties of surface-passivated Ni nanoparticles with mean diameters of approximately 14, 24, and 33.5 nm (see Figure 1A, C, F) were studied using a commercial SQUID magnetometer in the temperature range 2 K $\leq T \leq$ 370 K and a magnetic field up to 5 T, as exemplified in Figure 4A for the 33.5 nm particles. Figure 4B shows the zero-field-cooled (ZFC) and the field-cooled (FC) magnetization as a function of temperature for the 14 nm Ni nanoparticles deposited on a GaAs substrate. For ZFC measurement, the sample was cooled without an external magnetic field from 370 K down to 5

(32) Guo, L.; Liu, C.; Wang, R.; Xu, H.; Wu, Z.; Yang, S. *J. Am. Chem. Soc.* **2004**, *126*, 4530.
(33) Nikoobakht, B.; El-Sayed, M. A. *Langmuir* **2001**, *17*, 6368.
(34) Pérez-Juste, J.; Liz-Marzán, L. M.; Carnie, S.; Chan, D. Y. C.; Mulvaney, P. *Adv. Funct. Mater.* **2004**, *14*, 571.
(35) Anan'ev, A. V.; Boltoeva, M. Y.; Sukhov, N. L.; Bykov, G. L.; Ershov, B. G. *Radiochemistry* **2004**, *46*, 578.
(36) Wu, S.-H.; Chen, D.-H. *J. Colloid Interface Sci.* **2003**, *259*, 282.
(37) Kakkinidis, G.; Jannakoudakis, P. D. *J. Electroanal. Chem.* **1981**, *130*, 153.

K, followed by heating the sample in a magnetic field of 5 mT and measuring the magnetization. For FC measurements, the sample was cooled in a magnetic field of 5 mT from 370 to 5 K, and the magnetization was measured at 5 mT with increasing temperature.

The ZFC thermomagnetic curve shows a narrow peak at 16 K and a broad maximum at 140 K, whereas the FC magnetization decreases with increasing temperature. Above 170 K, the FC curve has the same quasi-linear temperature dependence as the ZFC curve. In the temperature range from 5 to 25 K, where the low-temperature peak in the ZFC thermomagnetic curve is observed, the FC magnetization decreases steeply. The narrow low-temperature ZFC peak at 16 K is also observed for the nanoparticles with average diameters of 24 and 33.5 nm. Above 50 K, the ZFC magnetization of both larger diameter samples increases monotonically up to 320 K and a shallow maximum might be identified at or above the highest measuring temperature of 370 K. Over the whole temperature range, the FC curve yields a larger magnetization and only approaches the value of the ZFC magnetization above 370 K. These measurements indicate the presence of several magnetic phases in the samples. We suppose that the low-temperature, size-independent peak in the ZFC curves is due to the presence of antiferromagnetic $Ni(OH)_2$ with a reduced Néel temperature T_N of approximately of 16 K, in comparison to bulk β-$Ni(OH)_2$ (T_N = 30 K). β-$Ni(OH)_2$ has a hexagonal layer structure of CdI_2 type and a metamagnetic transition at a critical field H_c = 0.5 T at 4.2 K.[38] The reduced Néel temperature can be explained by the finite size of the $Ni(OH)_2$ crystallites and/or the presence of defects as for example shown in references[39] and.[40] The broad peak at 140 K observed for the 14 nm Ni nanoparticles is due to the superparamagnetic transition of the ferromagnetic Ni nanoparticle core. The superparamagnetic blocking temperatures of the nanoparticles with diameters of 24 and 33.5 nm are above the available measurement temperature. These nanoparticles also show ferromagnetic open hysteresis loops at 300 K.

The position of the superparamagnetic maxima in the ZFC magnetization curve, T_{max}, does not necessarily coincide with the blocking temperature of the nanoparticles, T_B.[41] Both the distribution in particle sizes and the interaction between particles result in a shift of the maximum in the ZFC curve toward higher temperatures in comparison to the intrinsic T_B given by the anisotropy energy of the particle. The mean blocking temperature $\langle T_B \rangle$ for an ensemble of interacting magnetic particles is given by[42]

$$\langle T_B \rangle = \frac{K_{eff}\langle V_p \rangle + \varepsilon_D}{k_B \ln\left(\frac{t_m}{\tau_0}\right)}$$

where K_{eff} is the effective magnetic anisotropy energy density, $\langle V_p \rangle$ is the mean volume of the Ni core and k_B is the Boltzmann constant. $t_m \approx 100$ s is the observation time for dc SQUID measurements, and τ_0 is a microscopic relaxation time $\sim 1 \times 10^{-10}$ to 1×10^{-11} s. The effective dipolar interaction energy in an assembly of superparamagnetic particles ε_D is[43]

$$\varepsilon_D = \frac{\mu_0}{4\pi}\frac{\alpha \mu_p^2}{d^3}$$

where α is a constant given by the sum of all dipolar interactions among the particles, d is the average distance between neighboring dipoles, and μ_p is the magnetic moment of the Ni nanoparticle core. According to our TEM observation, the mean separation between neighboring nanoparticles due to the surfactant layer is 2.5−3 nm, and additionally the ferromagnetic cores are separated by the antiferromagnetic oxide shells. In the case of 14 nm oxidized particles, we estimate that the system is composed of ferromagnetic Ni nanoparticles embedded in matrix of antiferromagnetic NiO and surfactant, with a filling factor of ~0.08. Assuming the bulk magnetization value for the Ni core, one can estimate that the maximum magnetic dipolar interaction energy of the oxidized Ni nanoparticles is 1.7×10^{-21} J.

We find that K_{eff} is $\sim 1.2 \times 10^5$ J/m^3 for the 14 nm Ni/NiO nanoparticles with a mean diameter of 9 nm of the ferromagnetic core. This value is much larger than the magnetocrystalline anisotropy constant of fcc bulk Ni (1.2×10^4 J/m^3 at 4.2 K and 0.45×10^4 J/m^3 at 300 K). The enhancement of K_{eff} is due to the presence of the antiferromagnetic NiO shell (T_N(bulk) = 523 K). In ferromagnetic (FM) nanoparticles covered with antiferromagnetic (AFM) shells, the exchange anisotropy induced by exchange coupling at the FM/AFM interface can provide an extra source of anisotropy resulting in an increase of the effective magnetic anisotropy of the nanoparticles.[44–46] The presence of the unidirectional anisotropy is confirmed by the observation of the exchange bias effect: the hysteresis loop of the AFM/FM system which is cooled in a static magnetic field from a temperature above the Néel temperature but below the Curie temperature is shifted along the field axis generally in the opposite direction to the cooling field. A shift of the hysteresis loop has been observed when cooling was started at a temperature well below the Néel temperature of NiO or the Curie temperature of the ferrimagnet in the case of an oxidized Fe nanostructured system.[47,48] Reduced Néel temperatures have been observed in nanoparticle systems[49,50] and thin antiferromagnetic films,[51] while finite size effects in NiO nanoparticles were found to result in unusual 8-, 4-,

(38) Takada, T.; Bando, Y.; Kiyama, M.; Miyamoto, H.; Sato, T. *J. Phys. Soc. Jpn.* **1966**, *21*, 2745.
(39) Sorai, M.; Kosaki, A.; Suga, H.; Seki, S. *J. Chem. Thermodynamics* **1969**, *1*, 119.
(40) Enoki, T.; Tsujikawa, I. *J. Phys. Soc. Jpn.* **1978**, *45*, 1515.
(41) Antoniak, C.; Lindner, J.; Salgueiriño-Maceira, V.; Farle, M. *Phys. Status Solidi A* **2006**, *203*, 2968.
(42) Margeat, O.; Tran, M.; Spasova, M.; Farle, M. *Phys.Rev.B* **2007**, *75*, 134410.
(43) Allia, P.; Coisson, M.; Tiberto, P.; Vinai, F.; Knobel, M.; Novak, M. A.; Nunes, W. C. *Phys.Rev. B* **2001**, *64*, 144420.
(44) Wiedwald, U.; Lindner, J.; Spasova, M.; Frait, Z.; Farle, M. *Phase Transitions* **2005**, *78*, 85.
(45) Skumryev, V.; Stoyanov, S.; Zhang, Y.; Hadjipanayis, G.; Givord, D.; Nogués, J. *Nature* **2003**, *423*, 850.
(46) Li, S.; Liu, M.; Bi, H.; Lue, L.; Zou, W.; Huang, Z.; Du, Y. *J. Alloys Compd.* **2006**, *425*, 1.
(47) Löffler, J. F.; Meier, J. P.; Doudin, B.; Ansermet, J. Ph.; Wagner, W. *Phys. Rev. B* **1998**, *57*, 2915.
(48) Shavel, A.; Rodríguez-González, B.; Spasova, M.; Farle, M.; Liz-Marzán, L. M. *Adv. Funct. Mater.* **2007**, *17*, 3870.
(49) Ahmad, T.; Chopra, R.; Ramanujuchary, K. V.; Lofland, S. E.; Ganguli, A. K. *Solid State Sci.* **2005**, *7*, 891.
(50) Selbach, S. M.; Tybell, Th.; Einarsrud, M.-A.; Grande, T. *Chem. Mater.* **2007**, *19*, 6478.
(51) Ambrose, T.; Chien, C. L. *Phys. Rev. Lett.* **1996**, *76*, 1743.

or 4-sublattice spin configurations with relatively weak coupling between the sublattices.[52] At a rough ferromagnetic/antiferromagnetic interface, the existence of a disordered interface spin-glass-like magnetic phase with low freezing point has been discussed.[53,54]

The hysteresis loops of the oxidized 33.5 nm Ni nanoparticles measured at 2 K after ZFC and FC in applied magnetic field of 5 T from 320 to 2 K are shown in Figure 4A. A clear shift of the FC curves can be seen. For all samples we have observed the shift of the hysteresis loops opposite to the cooling-field direction. The values obtained for the exchange bias fields, $\mu_0 H_{eb}$, were 62.1, 26.4, and 21.4 mT at 2 K for the oxidized 14, 24, and 33.5 nm Ni nanoparticles, respectively. The interfacial exchange energy per unit area, σ, for spherical nanoparticles can be roughly estimated to be $\sigma = \mu_0 H_{eb} M_{FM} d_{FM}/6$ (M_{FM} is the volume magnetization of the FM nanoparticle core with a diameter of d_{FM}).[55] The factor 6 arises from the ratio of volume-to-surface area of the sphere. Assuming bulk Ni magnetization for the particle core and a thickness of the oxide shell of 2.5 nm we calculate within the error bars the same value of the interfacial exchange energy density for all particles, $\sigma = 0.048 \pm 0.004$ mJ/m^2. The exchange bias field decreases with increasing temperature and completely vanishes at 50 K for all nanoparticle sizes. At this temperature thermal disorder becomes dominant over the shell-induced magnetic unidirectional anisotropy.

Usually, field cooling of an FM/AFM system not only leads to the induced unidirectional magnetic anisotropy (shift of the hysteresis loop) but also to an increased uniaxial magnetic anisotropy, which becomes evident by a broadening of the hysteresis loop.[56,57] In the case when the AFM anisotropy is larger than the interfacial exchange interaction, the shift of the hysteresis loop, which is due to the presence of a magnetic phase whose moments cannot be reversed by the applied field, is observed. When the strength of the exchange anisotropy interaction is comparable to that of the AFM anisotropy, the broadening of the hysteresis loop is observed because of the contribution of a reversible interfacial phase.[58,] For the investigated oxidized Ni nanoparticles, we found almost no difference (less than 2%) between the coercivities of the ZFC and the FC magnetization curves. This is an indication for the AFM anisotropy being much larger than the interfacial exchange interaction.

Magnetic Interactions and Chain Formation. The ferromagnetic character of the obtained Ni nanoparticles was reflected not only on the magnetic characterization results, but also on the spontaneous formation of nanoparticle chains, presumably because of dipole−dipole interactions, both upon drying on solid surfaces and in solution. Detailed theoretical[60] and experimental[10,61,62] studies of such interactions between ferromagnetic particles have been reported in the past, which showed that dipolar interactions are very sensitive to particle size and to the concentration of particles in the colloid.[63]

In the present work, we initially observed that the larger Ni particles show magnetic dipole−dipole interaction, reflected in the spontaneous formation of nanoparticle chains when drying a drop of the colloid on carbon-coated TEM grids at 300 K, as shown in Figure 5A. The length and uniformity of the chains depends on the particle size, so that it decreases for smaller particles. Additionally, when a magnetic field of ca. 0.2 T was applied, alignment into long chain structures over large areas, through a magnetophoretic deposition process, was observed, as exemplified for the same (33 nm) particles in the TEM image of Figure 5B, and for smaller (27 nm) particles in the SEM images (colloid dried on a Si wafer) shown in Figure 5D and in the Supporting Information (Figure S5). Although the concentration of particles and the nature of the substrate was different in this case, we could observe chains that can span over several micrometers, together with eventual formation of Y-junctions.

Interestingly, in the absence of an external applied magnetic field, our Ni particles have been observed to still display magnetic dipole−dipole interactions indicated by the chain formation (Figure 5A). Zero-field interactions between particles have been studied in the context of a better understanding of the morphology and thermodynamics of dipolar fluids.[64] Zero-field dipolar interactions between nickel particles were also observed when dried on Si wafers, under conditions equal to those presented in Figure 5D, resulting in the formation of small trimer and tetramer chains, uniformly distributed on the surface (see the Supporting Information, Figure S6). This behavior is similar to previously reported results,[10] although it cannot be directly compared to the behavior of particles interacting in solution, since during the drying process on the substrate, the concentration of particles gradually increases as the solvent evaporates, thereby increasing dipole−dipole interactions. Philipse and co-workers showed that formation of dipolar chains in ferrolfluids could be directly observed by cryogenic electron microscopy.[63] To avoid time-consuming sample preparation and elevated cost of the mentioned microscopy technique, Pyun and co-workers showed that structures formed by interacting particles in solution could be alternatively "frozen" by in situ surface-polymerization process[65,66] or by the so-called fossilized liquid assembly (FLA) method[67]

(52) Kodama, R. H.; Makhlouf, S. A.; Berkowitz, A. E. *Phys. Rev. Lett.* **1997**, *79*, 1393.
(53) Kodama, R. H.; Berkowitz, A. E. *Phys. Rev. B* **1999**, *59*, 6321.
(54) Gruyters, M. *Phys. Rev. Lett.* **2005**, *95*, 077204/1.
(55) Nogués, J.; Schuller, I. K. *J. Magn. Magn. Mater.* **1999**, *192*, 203.
(56) Meiklejohn, W. H.; Bean, C. P. *Phys. Rev.* **1957**, *105*, 904.
(57) Spasova, M.; Wiedwald, U.; Farle, M.; Radetic, T.; Dahmen, U.; Hilgendorff, M.; Giersig, M. *J. Magn. Magn. Mater* **2004**, *272*−*276*, 1508.
(58) Soeya, S.; Nakamura, S.; Imagawa, T.; Narishige, S. *J. Appl. Phys.* **1995**, *77*, 5838.
(59) Nogués, J.; Sort, J.; Langlais, V.; Skumryev, V.; Suriñach, S.; Muñoz, J. S.; Baró, M. D. *Phys. Rep.* **2005**, *65*, 422.
(60) Camp, P. J.; Shelley, J. C.; Patey, G. N. *Phys. Rev. Lett.* **2000**, *84*, 115.
(61) Salgueiriño-Maceira, V.; Correa-Duarte, M. A.; Hucht, A.; Farle, M. *J. Magn. Magn. Mater.* **2006**, *303*, 163.
(62) Klokkenburg, M.; Dullens, R. P. A.; Kegel, W. K.; Erne, B. H.; Philipse, A. P. *Phys. Rev. Lett.* **2006**, *96*, 037203/1.
(63) Butter, K.; Bomans, P. H. H.; Frederik, P. M.; Vroege, G. J.; Philipse, A. P. *Nat. Mater.* **2003**, *2*, 88.
(64) Safran, S. A. *Nat. Mater.* **2003**, *2*, 71.
(65) Korth, B. D.; Keng, P.; Shim, I.; Bowles, S. E.; Tang, C.; Kowalewski, T.; Nebesny, K. W.; Pyun, J. *J. Am. Chem. Soc.* **2006**, *128*, 6562.
(66) Bowles, S. E.; Wu, W.; Kowalewski, T.; Schalnat, M. C.; Davis, R. J.; Pemberton, J. E.; Shim, I.; Korth, B. D.; Pyun, J. *J. Am. Chem. Soc.* **2007**, *129*, 8694.
(67) Benkoski, J. J.; Bowles, S. E.; Korth, B. D.; Jones, R. L.; Douglas, J. F.; Karim, A.; Pyun, J. *J. Am. Chem. Soc.* **2007**, *129*, 6291.

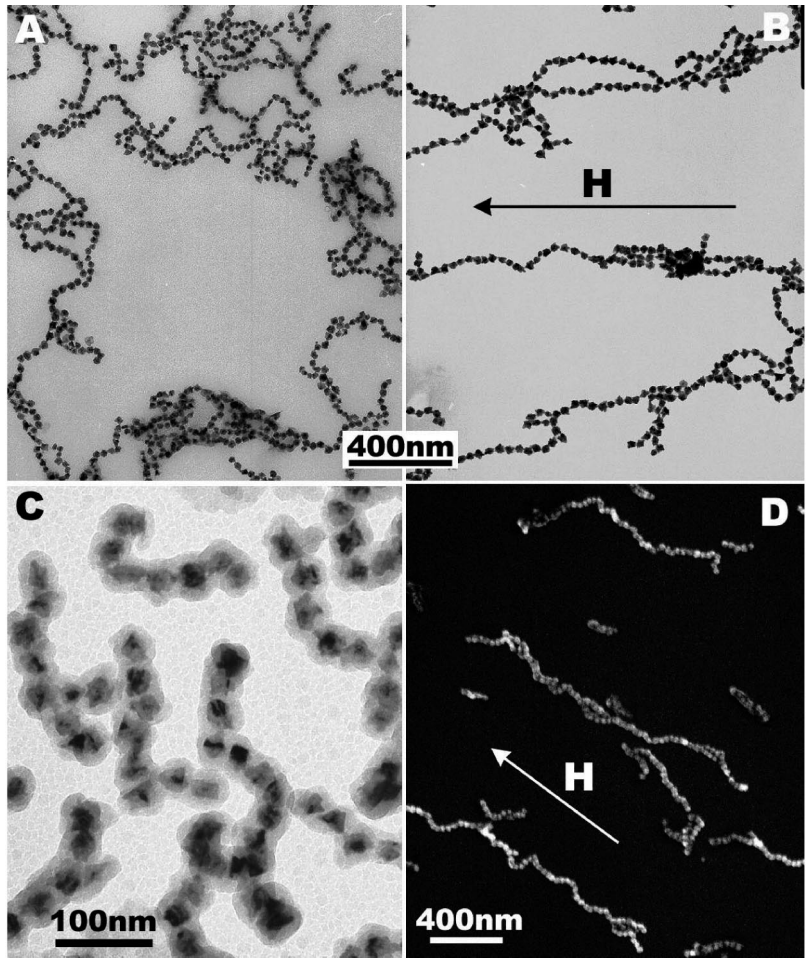

Figure 5. One-dimensional, chainlike assembly of nickel nanoparticles. (A) Zero-field linear assembly of 33 nm Ni on a TEM grid. (B) TEM image of long assemblies of 33 nm Ni under an external magnetic field (0.2 T). (C) TEM image of zero-field nanoparticle chains which are "fossilized" by coating with homogeneous silica shells. (D) SEM image of linear assemblies of Ni nanoparticles (27 nm) under an external magnetic field (0.2 T), on a Si wafer.

of chain-like assemblies of cobalt particles. Although the surface modification of ferromagnetic particles by amorphous silica in dilute solution[61,68] has been shown to lead to individual Co particles covered by silica shells, we show here that deposition of silica on our Ni particles leads to chainlike, quasi-one-dimensional structures, in which the chains formed by nickel particles in solution are fixed through slow silica precipitation, whereas the chains can be disrupted when the particles are smaller and the interactions are weaker, such as those reported for Co in refs[51] and.[58] An example of fossilized Ni nanoparticle chains, obtained through silica coating (using the method described in ref.[69]), is shown in Figure 5C, for particles with average diameter of 30 nm, coated with ca. 13 nm thick silica shells.

Conclusions

In summary, we have demonstrated that the catalytic activity of Pt seeds can be used for the uniform seeded growth, low-temperature reduction of nickel by hydrazine in aqueous CTAB solution, leading to size-controlled, surface-passivated Ni nanoparticles in a range between 13 and 33 nm, by simple variation of the amount of Pt seeds in the growth solution. Moreover, oxidized Ni nanoparticles show an increased magnetic effective anisotropy due to contribution of the size-independent interfacial exchange interaction (0.048 ± 0.004 mJ/m^2 at 2 K) at the Ni/NiO$_x$ interface in the particles. The exchange bias effect strongly decreases with increasing temperature and completely vanishes at 50 K for all particle sizes. Fourteen nanometer diameter particles are superparamagnetic at room temperature, whereas the nanoparticles with diameters larger than 24 nm show ferromagnetic behavior that leads to chain formation in the nanoparticle solution even in the absence of external magnetic field.

Acknowledgment. C. Serra (CACTI, U. Vigo) is thanked for carrying out XPS measurements, and J. Millos (CACTI, U. Vigo) for XRD analysis. This work was supported by the European Commission through the Marie Curie Research Training Network "SyntOrbMag", Contract MRTNCT-2004-005567, and the Spanish Ministerio de Ciencia e Innovación (Consolider-Ingenio 2010 project *Nanobiomed*).

Supporting Information Available: Additional information (PDF). This material is available free of charge via the Internet at http://pubs.acs.org.

CM800665S

(68) Kobayashi, Y.; Horie, M.; Konno, M.; Rodríguez-González, B.; Liz-Marzán, L. M. *J. Phys. Chem. B* **2003**, *107*, 7420.
(69) Pastoriza-Santos, I.; Sánchez-Iglesias, A.; García de Abajo, F. J.; Liz-Marzán, L. M. *Adv. Funct. Mater.* **2007**, *17*, 1443.